PCCP

PAPER

View Article Online
View Journal | View Issue

Check for updates

Cite this: *Phys. Chem. Chem. Phys.*, 2018, **20**, 10108

Framework flexibility of ZIF-8 under liquid intrusion: discovering time-dependent mechanical response and structural relaxation†

Yueting Sun,[ab] Yibing Li[b] and Jin-Chong Tan*[a]

Received 20th January 2018,
Accepted 9th March 2018

DOI: 10.1039/c8cp00447a

rsc.li/pccp

The structural flexibility of a topical zeolitic imidazolate framework with sodalite topology, termed ZIF-8, has been elucidated through liquid intrusion under moderate pressures (*i.e.* tens of MPa). By tracking the evolution of water intrusion pressure under cyclic conditions, we interrogate the role of the gate-opening mechanism controlling the size variation of the pore channels of ZIF-8. Interestingly, we demonstrate that its channel deformation is recoverable through structural relaxation over time, hence revealing the viscoelastic mechanical response in ZIF-8. We propose a simple approach employing a glycerol–water solution mixture, which can significantly enhance the sensitivity of intrusion pressure for the detection of structural deformation in ZIF-8. By leveraging the time-dependent gate-opening phenomenon in ZIF-8, we achieved a notable improvement (50%) in energy dissipation during multicycle mechanical deformation experiments.

1. Introduction

Zeolitic imidazolate frameworks (ZIFs) are a promising sub-family of microporous metal–organic frameworks (MOFs),[1,2] with a zeolitic network topology assembled from tetrahedral metal centers (MN_4, M = metal ions such as Zn^{2+} or Co^{2+}) bridged by imidazolate-based linkers.[3] Notably, many ZIF structures exhibit large pore cavities, but they are interconnected by narrow channels (*i.e.* window apertures) that allow size-selective separations.[4] Further to the tunable structure and functionality of ZIFs, they are advantageous over other MOFs due to enhanced chemical/thermal stability, which is a typical feature of conventional zeolites.[5] From the mechanical viewpoint, however, the open-framework structure of ZIFs is not as rigid as zeolites.[6,7] Indeed, their structural flexibility has drawn considerable attention since it may strongly affect their engineering performance[8,9] in applications such as gas separations, sensing, guest storage and delivery.[10–12]

ZIF-8 [$Zn(mIM)_2$, mIM = 2-methylimidazolate] is amongst the most investigated ZIFs due to its ease of synthesis coupled with a large surface area and excellent chemical stability.[11] ZIF-8 has a sodalite (SOD) topology with relatively narrow channels comprising 6-membered rings (window size $\sim$3.40 Å) connecting larger internal pores ($\sim$11.6 Å).[3] However, 'over-sized' molecules (such as methane, 3.8 Å and nitrogen, 3.64 Å)[13,14] can pass through these narrow channels, unveiling its structural flexibility attributed to the 'gate-opening' mechanism of ZIF-8. Gate opening in ZIF-8 involves a rotational swing effect of the labile imidazolate linkers,[15] which can be triggered by either guest adsorption,[16] mechanical pressure,[17] or an external electrical field.[18] An unconventional two-step isotherm observed in nitrogen adsorption at 77 K reveals that low gas pressures (0.2 and 2 kPa) lead to gate opening upon guest uptake.[16]

High-pressure diamond-anvil-cell compression (DAC) experiments have been conducted to study the structural and chemical changes in ZIF-8 up to 4 GPa using different pressure-transmitting media (PTM).[19] Using a small molecular sized penetrating (hydrophilic) liquid such as methanol and ethanol, there will be a reversible phase transition at 1.47 GPa; the high-pressure phase reorients the imidazolate linkers *via* the gate-opening mechanism, which increases the size of the narrow channels connecting the pores.[17] Whereas, if a non-penetrating fluid (*e.g.* Fluorinert) is used as the PTM or ZIF-8 is compressed without any PTM, irreversible structural transition and amorphization will occur as the pressure goes beyond 0.34 GPa.[20] However, another study with no PTM, utilizing *in situ* FTIR spectroscopy instead of X-ray diffraction, reported that ZIF-8 can be compressed reversibly within 1.6 GPa and further compression to 39 GPa will amorphize the structure.[21]

Despite all the foregoing efforts concerning the high pressure ($\sim$GPa) behavior of ZIF-8, its structural response under a

[a] *Multifunctional Materials & Composites (MMC) Laboratory, Department of Engineering Science, University of Oxford, Parks Road, Oxford OX1 3PJ, UK. E-mail: jin-chong.tan@eng.ox.ac.uk*

[b] *State Key Laboratory of Automotive Safety and Energy, Tsinghua University, Beijing, 100084, P. R. China*

† Electronic supplementary information (ESI) available: Experimental details, and XRD results of ZIF-8 before and after liquid intrusion tests, energy dissipation analysis. See DOI: 10.1039/c8cp00447a

moderate liquid intrusion pressure ($\sim$MPa) has just started to draw attention.[43] Moderate pressures of the order of several to tens of MPa ($\sim$10–100 bar) are central to engineering applications, for example in mechanical energy storage[22,23] and energy mitigation systems,[24,25] and for novel vehicle damping devices.[26–28] With a bulk modulus of 7.75 GPa for ZIF-8,[7] the structural distortion upon moderate pressure intrusion might be small (*e.g.*, a pressure of tens of MPa only creates a volumetric change of around 1%), thus giving us the unique opportunity to explore whether MPa pressure can be used to modify the flexible framework structure and molecular scale pore configurations in ZIF-8.

In this study, we propose a liquid-intrusion approach to study the variation of the pore channels of ZIF-8 when subjected to a moderate level of hydrostatic pressure in the MPa range. Instead of employing *in situ* XRD/FTIR techniques to track structural changes, we demonstrate the use of the penetrating liquid itself as a sensitive probe to detect the nanoscale variation of the channel size.

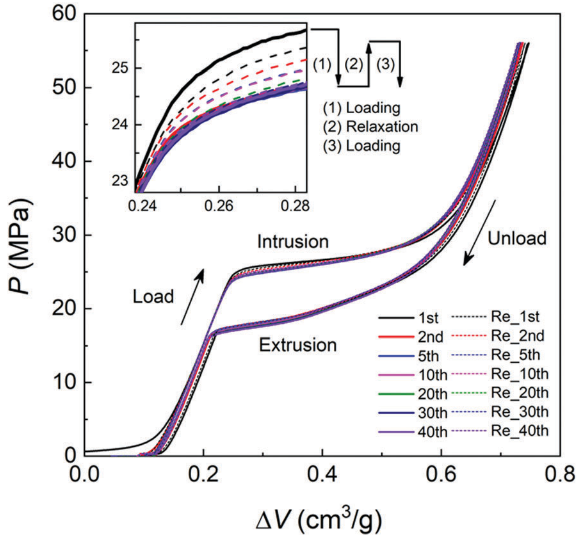

Fig. 1 P–ΔV curves of water intrusion into ZIF-8, including 40 consecutive loading–unloading cycles, and followed by another 40 cycles after a 24 hour relaxation time (dotted lines). The inset shows the transition curves at the start of water intrusion. Note that ΔV is negative due to compression.

2. Results and discussion

2.1 Water intrusion response under multi-cyclic loading

According to nanofluidics, non-wetting liquid will intrude nanopores at a critical pressure at which the capillary effect is exceeded, whereby this intrusion pressure is inversely proportional to the channel size.[29] Using this principle, we can characterize the pore size variation in ZIF-8 by monitoring the intrusion pressure of certain non-wetting liquids. Since ZIF-8 is inherently hydrophobic due to the presence of methyl functional groups,[30,31] it is convenient to begin by using water as the penetrating liquid. To demonstrate this concept, we fabricated a ZIF-8/water nanofluidic system, as depicted in Fig. S1 in the ESI.† ZIF-8 powder (Basolite Z1200 from BASF, XRD shown in Fig. S2, ESI†) and water were combined and sealed in a stainless-steel compression chamber. The pressure was induced by a 6 mm diameter piston inserted into the chamber driven by the Instron 5582 universal testing machine, which records force and displacement history during the loading and unloading cycles (up to 40). We applied a constant displacement rate of 0.5 mm min^{-1} and reversed the crosshead direction at a typical peak pressure of 56 MPa.

Fig. 1 shows the pressure *versus* volume change curves (P–ΔV) of ZIF-8, revealing its water intrusion response under the cyclic loading conditions. It can be seen that initially, as the pressure increases, the system volume decreases linearly, which is attributed to elastic compression of water and ZIF-8 particles, but without any pore intrusion due to its hydrophobicity. At $\sim$25 MPa, the capillary effect has been overcome and water molecules begin to intrude into the ZIF-8 pores. This intrusion process gives rise to a distinct plateau on the P–ΔV curve, which deviates from the elastic modulus of the system. When all the pore cavities have been occupied by water molecules, the plateau ends and another steep linear segment appears due to the compression of water and water-filled ZIF-8 crystals. The unloading curve has an extrusion plateau similar to the intrusion segment albeit at a relatively lower pressure down to $\sim$16 MPa, signifying that water molecules escape from ZIF-8 nanopores during decompression. It can be seen that the system recovers most of its initial volume when the applied pressure drops to zero. Though the water intrusion–extrusion phenomenon elucidated above is reminiscent of the work of Patarin and co-workers,[32,33] they have thus far reported the behavior of ZIF-8 for a much smaller number of deformation cycles (typically 3) and have not yet considered the influence of structural flexibility on the time-dependent mechanical response.

Due to the excellent water extrusion performance of ZIF-8, the consecutive 40 cycles in Fig. 1 exhibit almost overlapping P–ΔV curves. However, a closer examination of the data (see the inset of Fig. 1) unveils a more remarkable effect. Specifically, we have detected a subtle but measurable decline of $\sim$1 MPa in intrusion pressure upon consecutive multicycle loading. Furthermore, according to the results of another set of cyclic tests performed on the same sample after a 24 hour relaxation time, we found that this systematic decline can be recovered almost fully, and then declines again upon further cyclic loading. Because there should be no change in the solid–liquid interfacial properties among different cycles, we hypothesized that this systematic shift of intrusion pressure can be ascribed to the evolution of the window apertures leading into a ZIF-8 pore. That is, the narrow channels interconnecting the ZIF-8 pores have incrementally expanded in diameter due to water intrusion, therefore allowing water molecules to intrude at a lower pressure in the subsequent cycles. This phenomenon can be explained by the gate-opening mechanism prevalent in ZIF-8,[16,17,44] although previous experiments have not yet considered the effects of a large number of multicycle loading–unloading deformation. Herein, we established that there is a minor change measured in residual deformation (recoverable after structural relaxation), and a good retention of maximum volumetric change, where $\Delta V \sim 0.4\ cm^3\ g^{-1}$. Importantly, we also confirmed that the crystalline framework of ZIF-8 remains intact after multicycle mechanical loading, evidenced by the consistent intrusion plateau length further supported by the XRD data (Fig. S2 of ESI†) showing consistent relative Bragg peak intensities. The immersion in water does not create notable degradation of ZIF-8,[34] due to its high mass ratio to water (1 : 4) employed in this study.

2.2 Intrusion behavior of a glycerol–water solution mixture

Since the variation of water intrusion pressure observed in Section 2.1 is relatively subtle, we turn to another probe liquid whose molecular size is comparable to that of the ZIF-8 channels. In this way, the framework deformation can switch on and switch off the liquid intrusion and thus be easily detected. That is, the liquid molecules chosen should be slightly larger than the size of the ZIF-8 channels, so that they will intrude only after the framework has structurally deformed. To this end, glycerol is a good candidate, with its molecular size being 3.6 Å in the least extended dimension,[35] which is only slightly larger than the ZIF-8 channel with a limiting diameter of 3.4 Å. Notably, given that alcohol can have affinity with both water molecules and ZIF-8 frameworks, glycerol will promote water intrusion if it can enter the nanopores together with water molecules, while it will inhibit water intrusion if the channels are too narrow for glycerol molecules to enter. In light of this, compared with pure water intrusion into the ZIF-8 framework, we reasoned that the addition of glycerol into the liquid phase will (i) intensify the intrusion pressure prior to any structural deformation or (ii) diminish the intrusion pressure upon channel expansion. By implementing this approach, the sensitivity for the detection of structural changes of ZIF-8 can then be significantly improved.

We have demonstrated the efficacy of the above concept by systematically studying the intrusion behavior of a glycerol–water solution mixture into ZIF-8. Fig. 2 shows the cyclic P–ΔV curves with a glycerol concentration of 10 wt%. In the first cycle, the intrusion pressure has increased to 28 MPa, which is a 12% rise from the pure water intrusion value of 25 MPa. This finding indicates that glycerol is functioning as an intrusion inhibitor outside the ZIF-8 framework, due to its hydrogen bonding affinity with water molecules. Additional energy is thus required for the water molecules to dissociate themselves from glycerol–water clusters before they can enter the ZIF-8 pore channels. Furthermore, the data revealed that some liquid molecules are confined inside the ZIF-8 channels upon loading, which may expand the channels and facilitate the entry of glycerol molecules. This is supported by our data, whereby in the subsequent cycles, due to the intrusion promoting effect of glycerol, a lower plateau ($\sim$15 MPa) appears and then gradually becomes dominant with consecutive loading, while the initial plateau diminishes and finally disappears. The gap between these two plateaus is 13 MPa, which is a pronounced distinction

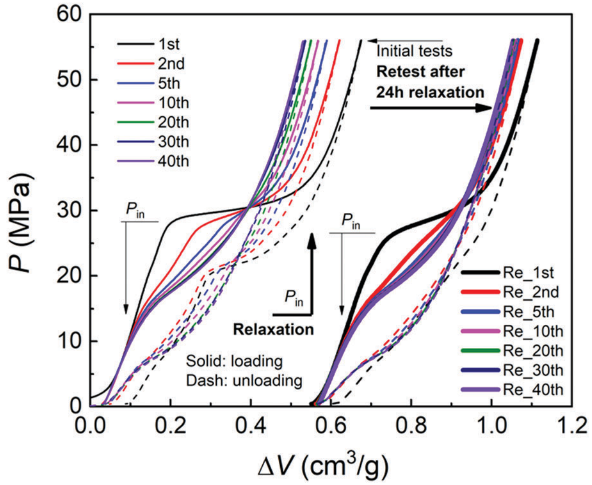

Fig. 2 P–ΔV curves of glycerol–water solution into the ZIF-8 framework, showing cyclic intrusion–extrusion curves of the 10 wt% glycerol–water system. Two sets of 40-cycle measurements were performed with a relaxation time of 24 h in between them. Note: retested curves shifted horizontally for clarity. Extrusion curves are shown as dotted lines. P_{in} denotes the intrusion pressure.

of intrusion pressure caused by framework deformation. Just like the case of pure water intrusion, the framework deformation is recoverable, which we have established by retesting the same sample after a relaxation period of 24 hours. Remarkably, we obtained the higher plateau again; this result is significant as it unambiguously proves that the ZIF-8 framework can undergo structural recovery over time. Likewise, we confirmed that subsequent multicycle reloading tests will reproduce the lower plateau again, as shown in Fig. 2.

2.3 Understanding glycerol concentration effects and intrusion characteristics of related polyhydric alcohols

For further validation, we have tested the effects of using different glycerol concentrations, as shown in Fig. 3(a). For the higher plateau characterized in the 1st cycle, the intrusion pressure has increased with glycerol concentration; while for the lower plateau shown in the 40th cycle, the intrusion pressure has decreased with glycerol concentration. This finding is consistent with the intrusion inhibiting and promoting mechanism of glycerol, both of which become stronger at higher concentrations. In the case of 50 wt% glycerol, we cannot detect the lower plateau because the intrusion pressure has declined to zero; this finding means that this binary liquid has become so hydrophilic that it spontaneously infiltrates the ZIF-8 nanopores.

We then investigated the effects of glycerol's neighbors by employing a series of polyhydric alcohols, encompassing ethylene glycol (C2), erythritol (C4) and xylitol (C5). The results are presented in Fig. 3(b). As expected, due to its smaller molecular size that can be accommodated by ZIF-8 channels without distortion, ethylene glycol serves as an intrusion promoter from the very start and thus lowers the intrusion pressure to 13 MPa. In contrast, erythritol and xylitol molecules are simply too big to infiltrate when being forced under pressure even after water intrusion and

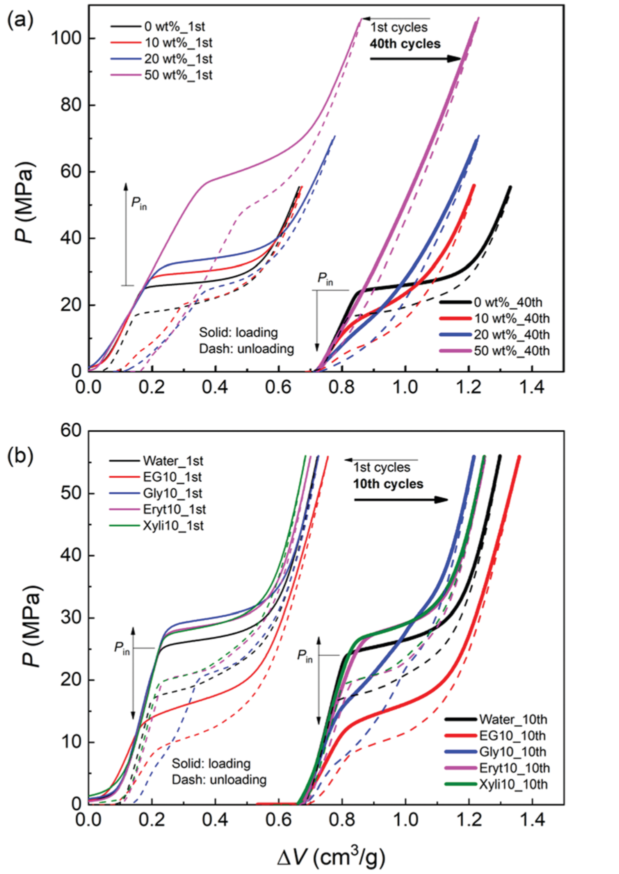

Fig. 3 Multicycle intrusion–extrusion curves of glycerol–water solution into the ZIF-8 framework. (a) Effects of glycerol concentration, with the higher plateau shown in the 1st cycle and the lower plateau shown in the 40th cycle. (b) Effects of alcohol type (at the same concentration 10 wt%), with the 1st and 10th cycles shown. Retested curves shifted horizontally for clarity.

subsequent framework deformation, therefore they act as intrusion inhibitors, resulting in higher plateaus for all the cycles. Unsurprisingly, as shown in Fig. 3(b), the lower plateau is hardly recognizable in the 10th cycle. By comparing with our results, we note that the incorporation of other small guest molecules into ZIF-8 pores has been achieved, for example caffeine,[36] through a slow diffusive process under extended solution stirring (without pressure) assisted by the structural flexibility of ZIF-8. In contrast, large guest molecules such as doxorubicin are far too large to penetrate the channels and only bind to the ZIF-8 surface,[37] whereas other bulky luminescent complexes can be entrapped within the pores of ZIF-8 using an *in situ* nanoconfinement strategy.[38]

2.4 Exploring the significance of mechanical deformation rate on the intrusion response of ZIF-8

By virtue of the proposed detection method, we are able to further explore the effects of the deformation rate on mechanical properties, which is an important question but not yet explored in MOFs due to limitations of the conventional techniques. Fig. 4 shows the intrusion of 10 wt% glycerol solution into ZIF-8 at a

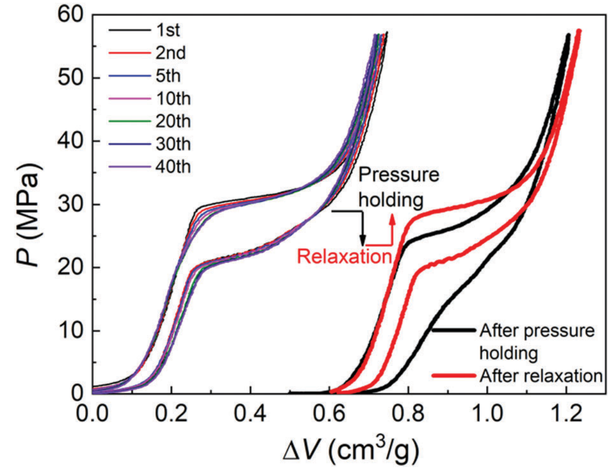

Fig. 4 P–ΔV curves of 10 wt% glycerol–water solution into the ZIF-8 framework at 50 mm min^{-1}, including 40 consecutive loading cycles, one following cycle after pressure holding at 56 MPa for 4 min, and a final cycle tested after a 24 h framework relaxation.

displacement rate of 50 mm min^{-1} (which is 100× greater than before). It is striking to see that the substantially higher intrusion rate produces almost identical P–ΔV curves in each cycle, with only a relatively small drop in intrusion pressure (*versus* the response shown in Fig. 2); this result suggests that glycerol molecules are residing outside the porous framework and thus functioning as intrusion inhibitors even after 40 cycles.

This is an interesting outcome, in contrast to the fact that glycerol molecules can enter the nanopores upon repeated cycles by low-rate intrusion (Fig. 2), here we discovered that the ZIF-8 framework deformation exhibits a strong strain-rate dependent effect. In this context, our data suggest that the channel deformation through the gate-opening mechanism takes time to occur, where the channel deforms gradually upon low-rate liquid intrusion and it needs continuous application of pressure to be fully triggered. To validate this rate effect, after the above cyclic loadings, the piston was held at the peak pressure (56 MPa) for 4 minutes to allow structural deformation to occur. Then, in the following loading cycle (still at 50 mm min^{-1}), we succeeded in obtaining a lower plateau at ∼24 MPa (which can recover after relaxation). Indeed, this result validated our conjecture that the gate-opening response of ZIF-8 is time-dependent and associated with the gradual deformation of its structural moieties, or, on the macroscale, this results in the rate-dependent 'viscoelastic' response of the ZIF-8 material.

3. Concluding remarks

In summary, we have elucidated a new method to probe the structural deformation of ZIF-8 at the molecular level, the approach is applicable to other MOF materials by adopting suitable non-wetting penetrating liquids. This study provides the evidence of ZIF-8 framework flexibility upon pressure-induced liquid intrusion, accommodated by a gate-opening mechanism. Specifically, we show that external pressures at tens of MPa prove to be capable of deforming the ZIF-8 framework, but without causing detrimental framework degradation when subjected to multicyclic loading. Our data revealed intriguing pore channel recovery through structural relaxation. We have discovered the viscoelasticity of the ZIF-8 framework by tracking the rate effects of its deformation under liquid intrusion conditions. Although it has been reported that the crystal size of ZIF-8 may influence the water intrusion pressure,[33] whether the framework flexibility and relaxation behavior of ZIF-8 are also size dependent when subjected to liquid intrusion remains to be established.

It is envisaged that our findings will not only open up the field of rate-dependent MOF mechanics,[39–41] but also lead to new MOF-based nanofluidic innovations.[22,42] For example, high-rate liquid intrusion performance is critical for applications like impact mitigators and shock absorbers afforded by nanoporous materials. To this end, we have calculated energy dissipations associated with liquid intrusion into ZIF-8 (Table S1, ESI†). Remarkably, we obtained up to $\sim$50% enhancement in energy dissipation upon multicycle loading (Fig. S3(c), ESI†) simply by exploiting the rate-sensitivity of ZIF-8; such a time-dependent gate-opening phenomenon in MOFs warrants further investigations using an even greater deformation strain rate.

Author contributions

Y. S. and J. C. T. conceived the project. Y. S. designed and performed the experiments. Y. S. analyzed the data with guidance from J. C. T. Y. S. and J. C. T. prepared the manuscript. All authors contributed to the discussion of results and have given approval to the final version of the manuscript.

Conflicts of interest

There are no conflicts to declare.

Acknowledgements

Y. Sun would like to thank the K. C. Wong Fellowship for funding this research. We thank Prof. Clive Siviour at Oxford University for helpful discussions concerning the mechanical response of rate-dependent materials. We are grateful to the ISIS Rutherford Appleton Laboratory, especially Dr Gavin Stenning and Dr Marek Jura at R53 Materials Characterization Laboratory for granting access to the XRD facilities. We thank Chengliang Xu for assistance in conducting the higher rate intrusion tests.

References

1 M. D. Allendorf and V. Stavila, *CrystEngComm*, 2015, **17**, 229–246.
2 J. C. Tan and B. Civalleri, *CrystEngComm*, 2015, **17**, 197–198.
3 A. Phan, C. J. Doonan, F. J. Uribe-Romo, C. B. Knobler, M. O'Keeffe and O. M. Yaghi, *Acc. Chem. Res.*, 2010, **43**, 58–67.
4 R. Banerjee, A. Phan, B. Wang, C. Knobler, H. Furukawa, M. O'Keeffe and O. M. Yaghi, *Science*, 2008, **319**, 939–943.
5 K. S. Park, Z. Ni, A. P. Cote, J. Y. Choi, R. D. Huang, F. J. Uribe-Romo, H. K. Chae, M. O'Keeffe and O. M. Yaghi, *Proc. Natl. Acad. Sci. U. S. A.*, 2006, **103**, 10186–10191.
6 J. C. Tan, T. D. Bennett and A. K. Cheetham, *Proc. Natl. Acad. Sci. U. S. A.*, 2010, **107**, 9938–9943.
7 J. C. Tan, B. Civalleri, C. C. Lin, L. Valenzano, R. Galvelis, P. F. Chen, T. D. Bennett, C. Mellot-Draznieks, C. M. Zicovich-Wilson and A. K. Cheetham, *Phys. Rev. Lett.*, 2012, **108**, 095502.
8 J. C. Tan and A. K. Cheetham, *Chem. Soc. Rev.*, 2011, **40**, 1059–1080.
9 N. C. Burtch, J. Heinen, T. D. Bennett, D. Dubbeldam and M. D. Allendorf, *Adv. Mater.*, 2017, 1704124, DOI: 10.1002/adma.201704124.
10 L. Diestel, N. Y. Wang, B. Schwiedland, F. Steinbach, U. Giese and J. Caro, *J. Membr. Sci.*, 2015, **492**, 181–186.
11 C. Zhang and W. J. Koros, *J. Phys. Chem. Lett.*, 2015, **6**, 3841–3849.
12 C. Gucuyener, J. van den Bergh, J. Gascon and F. Kapteijn, *J. Am. Chem. Soc.*, 2010, **132**, 17704–17706.
13 W. Zhou, H. Wu, M. R. Hartman and T. Yildirim, *J. Phys. Chem. C*, 2007, **111**, 16131–16137.
14 Q. Song, S. K. Nataraj, M. V. Roussenova, J. C. Tan, D. J. Hughes, W. Li, P. Bourgoin, M. A. Alam, A. K. Cheetham, S. A. Al-Muhtaseb and E. Sivaniah, *Energy Environ. Sci.*, 2012, **5**, 8359–8369.
15 M. R. Ryder, B. Civalleri, T. D. Bennett, S. Henke, S. Rudić, G. Cinque, F. Fernandez-Alonso and J. C. Tan, *Phys. Rev. Lett.*, 2014, **113**, 215502.
16 D. Fairen-Jimenez, S. A. Moggach, M. T. Wharmby, P. A. Wright, S. Parsons and T. Duren, *J. Am. Chem. Soc.*, 2011, **133**, 8900–8902.
17 S. A. Moggach, T. D. Bennett and A. K. Cheetham, *Angew. Chem., Int. Ed.*, 2009, **48**, 7087–7089.
18 A. Knebel, B. Geppert, K. Volgmann, D. I. Kolokolov, A. G. Stepanov, J. Twiefel, P. Heitjans, D. Volkmer and J. Caro, *Science*, 2017, **358**, 347–351.
19 J. Im, N. Yim, J. Kim, T. Vogt and Y. Lee, *J. Am. Chem. Soc.*, 2016, **138**, 11477–11480.
20 K. W. Chapman, G. J. Halder and P. J. Chupas, *J. Am. Chem. Soc.*, 2009, **131**, 17546–17547.
21 Y. Hu, H. Kazemian, S. Rohani, Y. N. Huang and Y. Song, *Chem. Commun.*, 2011, **47**, 12694–12696.
22 G. Fraux, F. X. Coudert, A. Boutin and A. H. Fuchs, *Chem. Soc. Rev.*, 2017, **46**, 7421–7437.
23 F. B. Surani, X. Kong, D. B. Panchal and Y. Qiao, *Appl. Phys. Lett.*, 2005, **87**, 163111.
24 Y. Sun, Z. Guo, J. Xu, X. Xu, C. Liu and Y. Li, *Mater. Des.*, 2015, **66**, 545–551.
25 Y. Sun, X. Xu, C. Xu, Y. Qiao and Y. Li, *Sci. Rep.*, 2016, **6**, 26694.
26 P. G. Yot, Z. Boudene, J. Macia, D. Granier, L. Vanduyfhuys, T. Verstraelen, V. Van Speybroeck, T. Devic, C. Serre, G. Ferey, N. Stock and G. Maurin, *Chem. Commun.*, 2014, **50**, 9462–9464.

27 C. V. Suciu and K. Yaguchi, *Exp. Mech.*, 2008, **49**, 383–393.
28 C. V. Suciu, T. Iwatsubo and S. Deki, *J. Colloid Interface Sci.*, 2003, **259**, 62–80.
29 Y. Qiao, L. Liu and X. Chen, *Nano Lett.*, 2009, **9**, 984–988.
30 K. Zhang, R. P. Lively, M. E. Dose, A. J. Brown, C. Zhang, J. Chung, S. Nair, W. J. Koros and R. R. Chance, *Chem. Commun.*, 2013, **49**, 3245–3247.
31 A. U. Ortiz, A. P. Freitas, A. Boutin, A. H. Fuchs and F. X. Coudert, *Phys. Chem. Chem. Phys.*, 2014, **16**, 9940–9949.
32 G. Ortiz, H. Nouali, C. Marichal, G. Chaplais and J. Patarin, *J. Phys. Chem. C*, 2014, **118**, 7321–7328.
33 I. Khay, G. Chaplais, H. Nouali, C. Marichal and J. Patarin, *RSC Adv.*, 2015, **5**, 31514–31518.
34 H. Zhang, D. Liu, Y. Yao, B. Zhang and Y. S. Lin, *J. Membr. Sci.*, 2015, **485**, 103–111.
35 L. Y. Chen, *J. Struct. Biol.*, 2013, **181**, 71–76.
36 N. Liedana, A. Galve, C. Rubio, C. Tellez and J. Coronas, *ACS Appl. Mater. Interfaces*, 2012, **4**, 5016–5021.
37 I. B. Vasconcelos, T. G. da Silva, G. C. G. Militao, T. A. Soares, N. M. Rodrigues, M. O. Rodrigues, N. B. da Costa, R. O. Freire and S. A. Junior, *RSC Adv.*, 2012, **2**, 9437–9442.
38 A. K. Chaudhari, M. R. Ryder and J. C. Tan, *Nanoscale*, 2016, **8**, 6851–6859.
39 Z. Su, W. L. Shaw, Y. R. Miao, S. You, D. D. Dlott and K. S. Suslick, *J. Am. Chem. Soc.*, 2017, **139**, 4619–4622.
40 K. Banlusan and A. Strachan, *J. Phys. Chem. C*, 2016, **120**, 12463–12471.
41 Z. Zeng and J. C. Tan, *ACS Appl. Mater. Interfaces*, 2017, **9**, 39839–39854.
42 P. G. Yot, L. Vanduyfhuys, E. Alvarez, J. Rodriguez, J.-P. Itié, P. Fabry, N. Guillou, T. Devic, I. Beurroies, P. L. Llewellyn, V. Van Speybroeck, C. Serre and G. Maurin, *Chem. Sci.*, 2016, **7**, 446–450.
43 Y. Grosu, G. Renaudin, V. Eroshenko, J. M. Nedelec and J. P. Grolier, *Nanoscale*, 2015, **7**, 8803–8810.
44 Y. Grosu, S. Gomes, G. Renaudin, J. P. E. Grolier, V. Eroshenko and J. M. Nedelec, *RSC Adv.*, 2015, **5**, 89498–89502.